



---

# Multivariate Geostatistical Analysis of CPT Readings for Reliable 3D Subsoil Modeling of Heterogeneous Alluvial Deposits in Padania Plain

**Diego Di Curzio**, Assistant Researcher, University “G. d’Annunzio” Chieti-Pescara (Chieti, Italy); email: [diego.dicurzio@unich.it](mailto:diego.dicurzio@unich.it)

**Giovanna Vessia**, Assistant Professor, University “G. d’Annunzio” Chieti-Pescara (Chieti, Italy); email: [g.vessia@unich.it](mailto:g.vessia@unich.it)

**ABSTRACT:** *Urban planning and big infrastructure designing demand two novel and seemingly contrasting approaches: 1) a continuous description of subsoil nature and behavior under natural hazards, to increase the resilience of urban areas; and 2) a reliable characterization of subsoil hydro-mechanical properties and monitoring their working behavior. Both exigences can be addressed by reconstructing 3D mechanical models at a local scale by extracting from large databases several in-situ testings, already available for several urbanized territories worldwide. In this paper, 182 cone tip resistance  $q_c$ , sleeve friction  $f_s$ , and pore pressure  $u_2$  profiles, drawn from CPTs performed in the Bologna district (Padania Plain, Italy), have been used. Here, the alluvial deposits are mixtures of silt, clay, and sands, and they locally show gravel lenses where the ancient fans from the Apennines can be detected. Their heterogeneous hydro-mechanical characters cannot be described only through point investigations such as CPTs. Additionally, the variability of these mechanical profiles and the uncertainties due to the limited amount of data must be assessed and used in designing and hazard mapping. Thus, to draw a continuous 3D subsoil mechanical model based on these 182 CPTs, the Partially Heterotopic Co-Kriging technique (PHCK) has been applied. This approach is a multivariate technique that can be used when only some measurements are taken at the same locations. It allows for the estimation of the distribution of  $q_c$ ,  $f_s$ , and  $u_2$  values in the studied domain by considering the spatial variability of the preceding random functions but also their spatial correlations. Differences in variance and spatial resolution between the measurements on the horizontal plane and along the vertical direction were accounted for by considering anisotropic spatial dependence models. As a result, this study has provided horizontal maps and vertical sections of  $q_c$ ,  $f_s$ , and  $u_2$ , as well as their 3D solid models.*

**KEYWORDS:** Multivariate geostatistics, Partially Heterotopic Co-Kriging technique, Padania Plain, 3D mechanical model, Italian geodatabase, CPT readings.

**SITE LOCATION:** [Geo-Database](#)

## INTRODUCTION

A common need for infrastructure designing and urban planning is the subsurface investigation of soil and rock formations to retrieve data about their litho-technical properties and substrata geometries. The ability to reconstruct 3D subsoil models of large portions of territory (at an urban scale or smaller) serves as a profitable tool for several engineering and urbanistic tasks. Furthermore, when the models get larger, it is essential to consider the variability of soil and rock properties in terms of spatial variability structure. Both these exigences can be addressed through the geostatistical approach applied to spatial numerical and categorical subsoil datasets even coming from different measurement sources (Vessia et al., 2020a). In this research, the case study of the Bologna province, located in Padania Alluvial Plain (Northern Italy), has been illustrated (Figure 1). These mixtures of silts, clays, and sands have been investigated through 182 cone penetration tests CPTus to generate a 3D litho-hydro-technical model of the first 30 m depth. These CPTus cover an area of 900 km<sup>2</sup>. The dataset used in this study has been selected from a large database implemented by the Regional Office for Territorial Protection and Development (<http://geoportale.regione.emilia-romagna.it/it>) of the Emilia-Romagna Region. Although the study area is

Submitted: 31 October 2020; Published: 25 October 2021

Reference: Di Curzio D., and Vessia G. (2021). Multivariate Geostatistical Analysis of CPT Readings for Reliable 3D Subsoil Modeling of Heterogeneous Alluvial Deposits in Padania Plain. International Journal of Geoengineering Case Histories, Volume 6, Issue 4, pp. 17-34, doi: 10.4417/IJGCH-06-04-02



expansive, the elevation differences among the different investigated sites do not exceed the order of a few tens of meters. Thus, in the attached database, the elevation related to each CPTu is not reported. Instead, vertical coordinates of the measurements correspond to their depth.

The method used to generate a reliable subsoil model based on cone tip resistance  $q_c$ , sleeve resistance  $f_s$ , and pore water pressure  $u_2$  was the Partially Heterotopic Co-Kriging technique (PHCK). This technique enables the creation of a continuous model of data that can be used both for planning activity if related to the territory within the urban borders, and for designing structures or infrastructures within the considered portion of modeled subsoil. When needed, additional investigations can be added not only to improve the reliability of the estimated model but also to increase the spatial resolution. To describe the CPTus as individual investigations, three clusters have been selected from Figure 1, each made up of four profiles of  $q_c$ ,  $u_2$ , and  $f_s$ . They have been characterized by means of Robertson's soil behavior type index and individual profiles along with depth, as described further below.

## GEO-LITHOTECHNICAL SETTING

### Geological features

The selected study area is about 900 km<sup>2</sup> wide and is located in the southern portion of Padania Plain, which is the largest alluvial plain throughout the Italian territory (about 46,000 km<sup>2</sup> wide). From a geological point of view, this is a tectonic depression that originated from the collision between the Southern Alps system and the Apennines system during the Plio-Pleistocene Age. It is filled by hundreds of meter thick deposits, that are related both to continental and marine deposition (Pieri and Groppi, 1981; Amorosi and Farina, 1995; Regione Emilia-Romagna and ENI-AGIP, 1998; ISPRA, 2009a, 2009b). These deposits appear highly heterogeneous, that is which is attributable to a combination of tectonic activity and climatic changes during the last hundreds of thousands of years (i.e., the Pliocene-Quaternary Age). In the study area, as clearly shown by the lithological cross-sections in Figure 2 (modified after ISPRA, 2009a, 2009b), alluvial deposits are characterized by predominant undifferentiated mixtures of silts and fine sands (i.e., flooding plain deposits) with both coarser and finer inclusions. Near the Apennines at the south, these inclusions are mainly large gravelly-sandy alluvial fans (see cross-section S1), while northward they become narrower sandy paleo-channels (i.e., fluvial deposits) and silty-clayey lenses (i.e., lacustrine deposits). As widely known, continental deposition, especially related to rivers and lakes, creates patterns of lithotypes that cannot be easily predicted (Vessia et al., 2020a), either in terms of lithologies or in volume and shape. Figure 3 shows the CPTu locations within the calculated 3D solid volume.

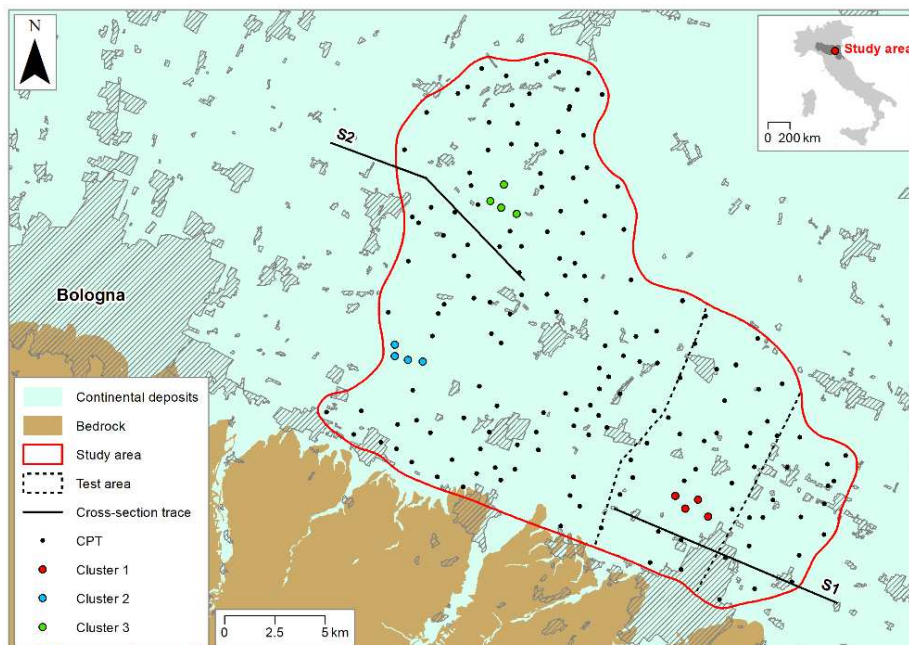


Figure 1. Geo-lithological map of the study area. The CPTu locations, the lithological cross-sections' traces (Figure 2), and the different clusters described below in the text (Figures 4, 5, 6, and 7) are shown.

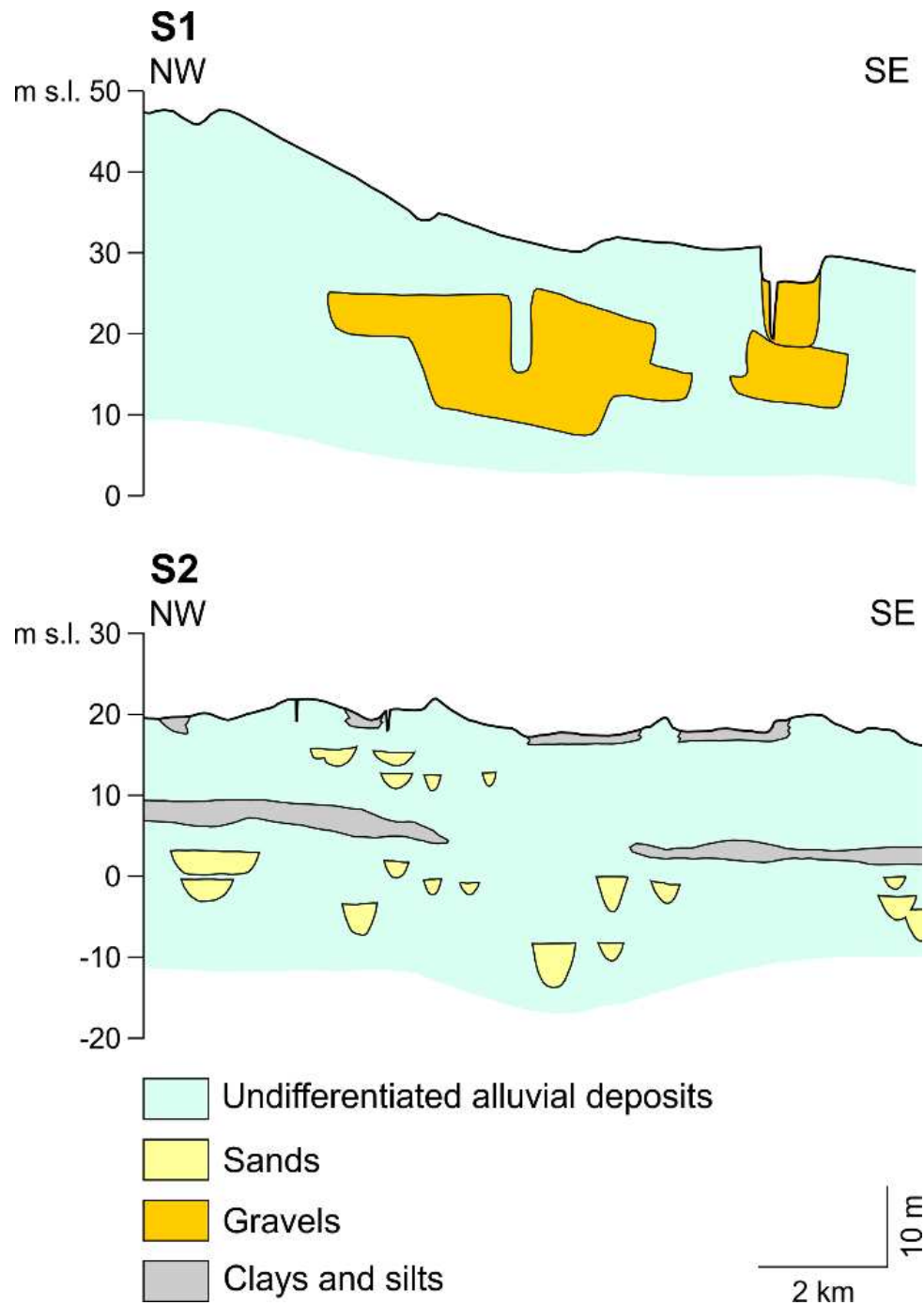


Figure 2. Lithological cross-sections of the study area (modified after ISPRA 2009a, 2009b).

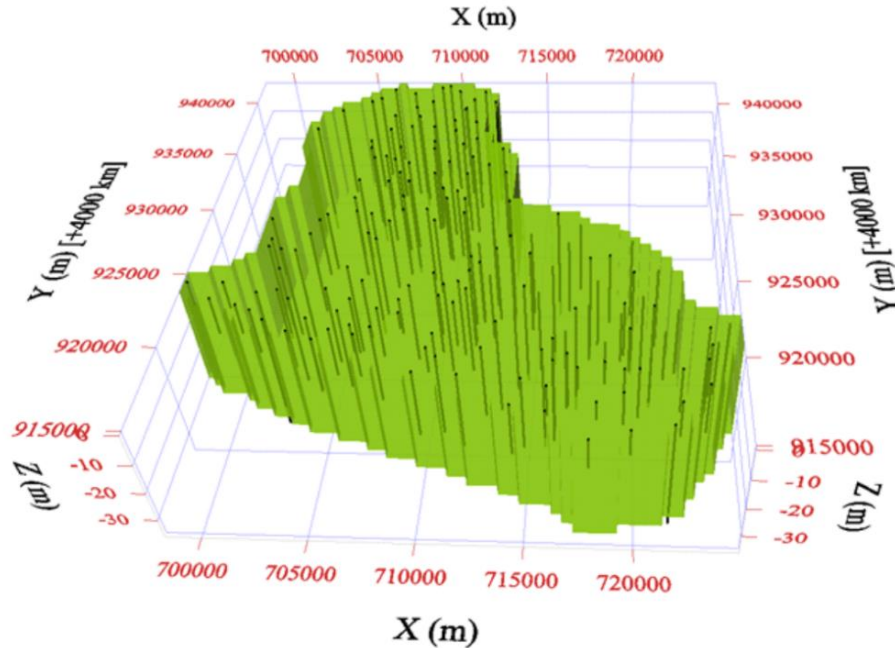


Figure 3. 182 CPT locations within the modeled volume of this study.

### Lithotechnical Characters

At first, insights into the soil behavior type index  $I_{SBT}$  proposed by Robertson (1990) and updated by Robertson (2009) have been shown. There,  $I_{SBT}$  domains have been calculated according to the following formula and the classes listed in Table 1.

$$I_{SBT} = \left[ (3.47 - \log(Q_t))^2 + (\log F_R + 1.22)^2 \right]^{0.5} \quad (1)$$

where  $R_f$  is the friction ratio  $= \frac{f_s}{q_c} \cdot 100\%$ ;  $Q_m$  is the normalized tip resistance  $Q_t = \left( \frac{q_t - \sigma'_{v0}}{\sigma'_{v0}} \right)$  and the terms inside this expression are:

$$q_t = q_c - u_2 \cdot (1 - a) \quad (2)$$

where the average value of  $a$  is 0.8. In addition,  $q_c$  is the tip resistance, while  $f_s$  is sleeve friction.

Data (green and red squares) from the three CPTu clusters selected in Figure 1 can be seen. Figure 3 shows the heterogeneous lithological nature of these sediments, ranging from 3 to 6 (see Table 1), typical of not layered soils. The  $I_{SBT}$  values reveal that a large part of the CPT measures falls into Class 4, which are sandy silts to silty sands, characterized by an increasing OCR and age; this may be due to the formation processes of these alluvial sediments and to the tectonic activity of the area.

Table 1. CPT Soil Behavior Type (SBT) (Robertson, 1990; updated by Robertson, 2009)

| Soil behavior type                        | $I_{SBT}$ | Class |
|-------------------------------------------|-----------|-------|
| Organic soils – clay                      | >3.6      | 7     |
| Clays – silty clay to clay                | 2.95-3.6  | 6     |
| Silt mixtures – clayey silt to silty clay | 2.60-2.95 | 5     |
| Sand mixtures – silty sand to sandy silt  | 2.05-2.60 | 4     |
| Sands – clean sand to silty sand          | 1.31-2.05 | 3     |
| Gravelly sand to dense sand               | <1.31     | 2     |

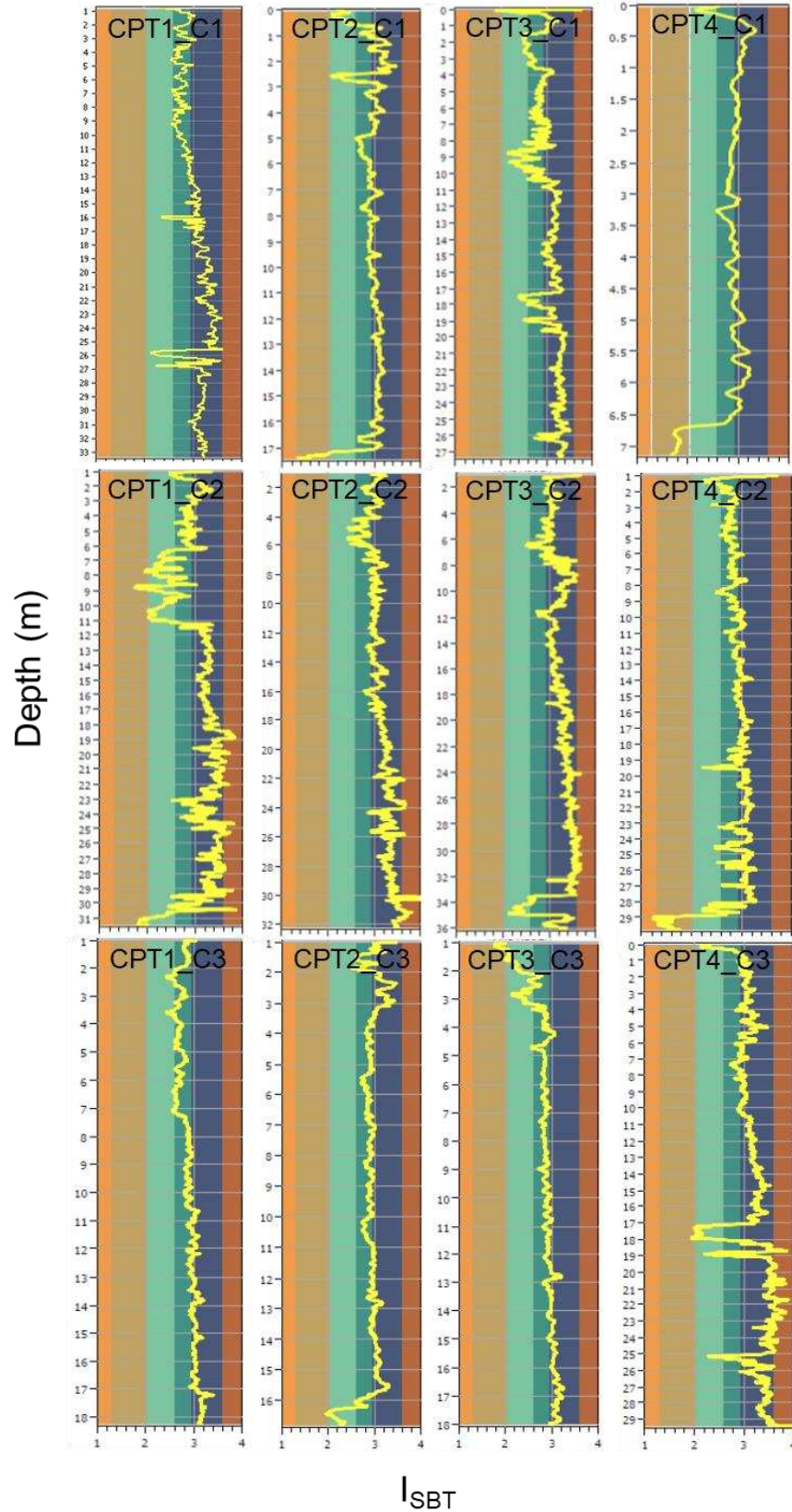


Figure 4. Robertson's SBT index  $I_{SBT}$  values (Robertson, 1990; updated by Robertson, 2009) related to data from the CPTus Cluster 1, 2, and 3 (see Fig. 1) (CLiQ v.3.0 - <https://geologismiki.gr/products/cliq>).



Looking at the profiles of  $q_c$ ,  $f_s$ , and  $u_2$  in Figures 5-7 from the three clusters, the heterogeneous character of the investigated alluvial deposits shown in Robertson's  $I_{SBT}$  has been confirmed. It is evident in the three sets of measurements at a short distance (hundreds of meters). Additionally, the individual  $q_c$ ,  $u_2$ , and  $f_s$  profiles allow some new insights. Figure 5 shows somewhere the absence of  $u_2$  measurements that can be replaced by the interpolated values calculated through the applied PHCK method. Furthermore, not all the CPTs have the same investigation depths. It frequently happens when CPTs from different campaigns must be used. Again, the PHCK method applied to all the 182 profiles enables us to overcome the lacking measures. Table 2 summarizes the elementary statistics on the three clusters of data. The means values of  $q_c$ ,  $u_2$ , and  $f_s$  seem to be similar, but the minima and the maximum values differ the most. The number of the measured values change for every cluster, and the skewness (S) and the kurtosis (K) of each cluster highlight the differences in the sample distributions among and within the three clusters. CPTu measures taken as samples of the whole dataset highlight how much cumbersome it would be to: 1) get a clear deterministic subsoil characterization from such a large dataset where the profiles that have been drilled hundreds of meters' distance are not placed in a regular grid and do not show similar subsoil characters, and 2) investigate the soil at different depths. These aspects of the studied measurements can be straightforwardly handled through geostatistics, especially the PHCK technique. The latter, as all the geostatistical techniques, provides continuous estimates and the related uncertainty within the entire investigated domain within the considered CPTs.

Table 2. Descriptive statistics of  $q_c$ ,  $u_2$  and  $f_s$ , related to: C1) Cluster 1, C2) Cluster 2, and C3) Cluster 3, where 25th=first quartile; 75th=third quartile; S=skewness; and K=kurtosis.

| C1)   |      |        |       |        |                  |        |                  |        |       |         |
|-------|------|--------|-------|--------|------------------|--------|------------------|--------|-------|---------|
|       | Unit | # data | Mean  | Min    | 25 <sup>th</sup> | Median | 75 <sup>th</sup> | Max    | S     | K       |
| $q_c$ | MPa  | 3893   | 2.120 | 0.090  | 1.370            | 1.770  | 2.320            | 35.950 | 8.947 | 103.156 |
| $u_2$ | MPa  | 2171   | 0.274 | -0.057 | 0.070            | 0.214  | 0.350            | 1.480  | 1.685 | 3.195   |
| $f_s$ | MPa  | 3893   | 0.092 | 0.001  | 0.056            | 0.081  | 0.112            | 0.521  | 1.898 | 5.542   |
| C2)   |      |        |       |        |                  |        |                  |        |       |         |
|       | Unit | # data | Mean  | Min    | 25 <sup>th</sup> | Median | 75 <sup>th</sup> | Max    | S     | K       |
| $q_c$ | MPa  | 6271   | 2.426 | 0.270  | 1.440            | 1.760  | 2.240            | 42.150 | 7.010 | 58.267  |
| $u_2$ | MPa  | 6271   | 0.361 | -0.100 | 0.084            | 0.322  | 0.556            | 1.947  | 0.656 | 0.114   |
| $f_s$ | MPa  | 6271   | 0.100 | 0.010  | 0.067            | 0.091  | 0.123            | 0.504  | 1.910 | 7.207   |
| C3)   |      |        |       |        |                  |        |                  |        |       |         |
|       | Unit | # data | Mean  | Min    | 25 <sup>th</sup> | Median | 75 <sup>th</sup> | Max    | S     | K       |
| $q_c$ | MPa  | 3968   | 2.304 | 0.320  | 1.470            | 2.155  | 2.735            | 15.360 | 3.984 | 24.787  |
| $u_2$ | MPa  | 3968   | 0.301 | -0.233 | 0.096            | 0.237  | 0.458            | 1.461  | 0.886 | 0.245   |
| $f_s$ | MPa  | 3968   | 0.128 | 0.004  | 0.078            | 0.121  | 0.171            | 0.525  | 0.714 | 0.663   |

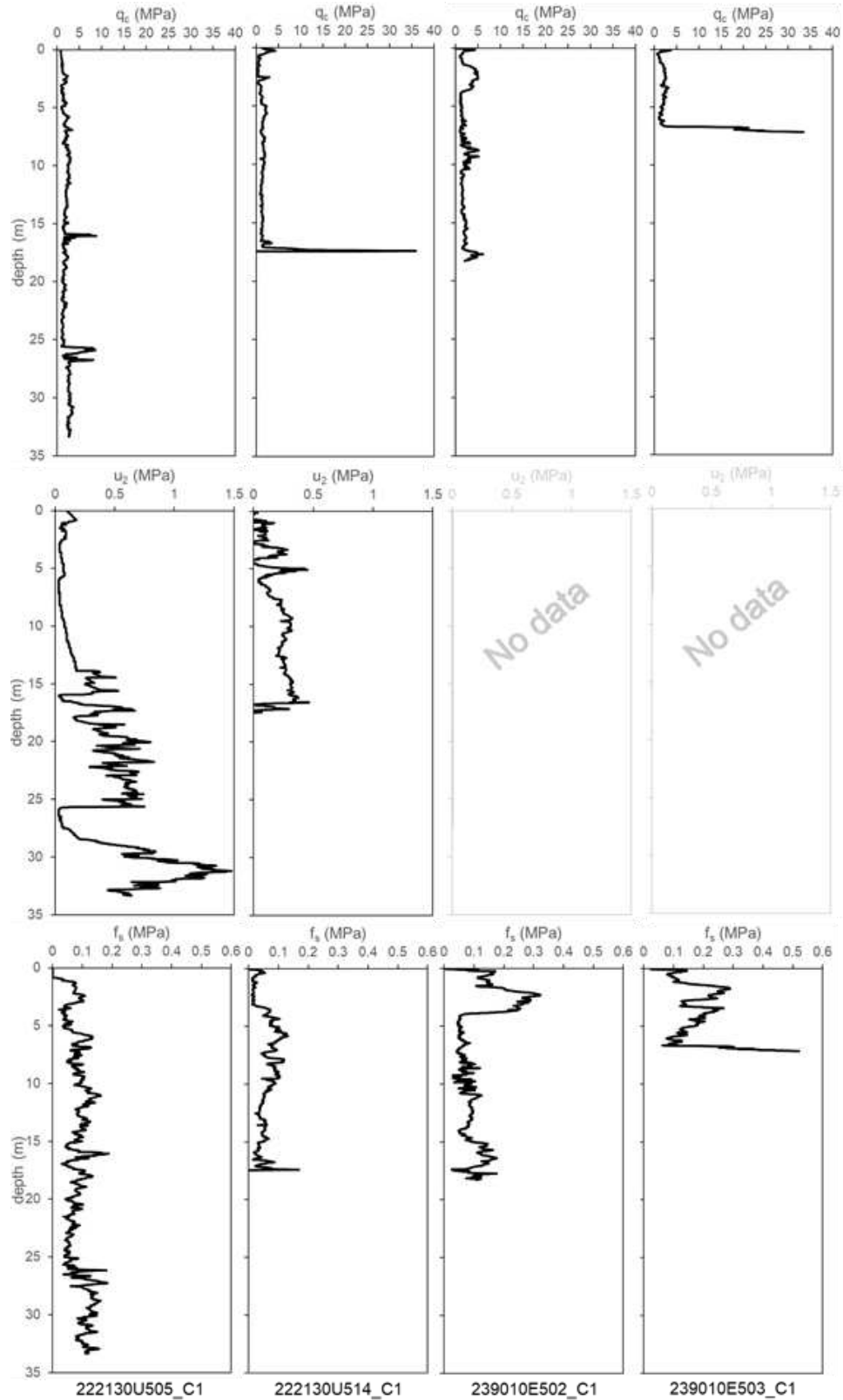


Figure 5. CPTu profiles ( $q_c$ ,  $u_2$ , and  $f_s$ ) related to Cluster 1 in Figure 1. From left to right: 222130U505, 222130U514, 239010E502, and 239010E503 CPTus in the attached database.

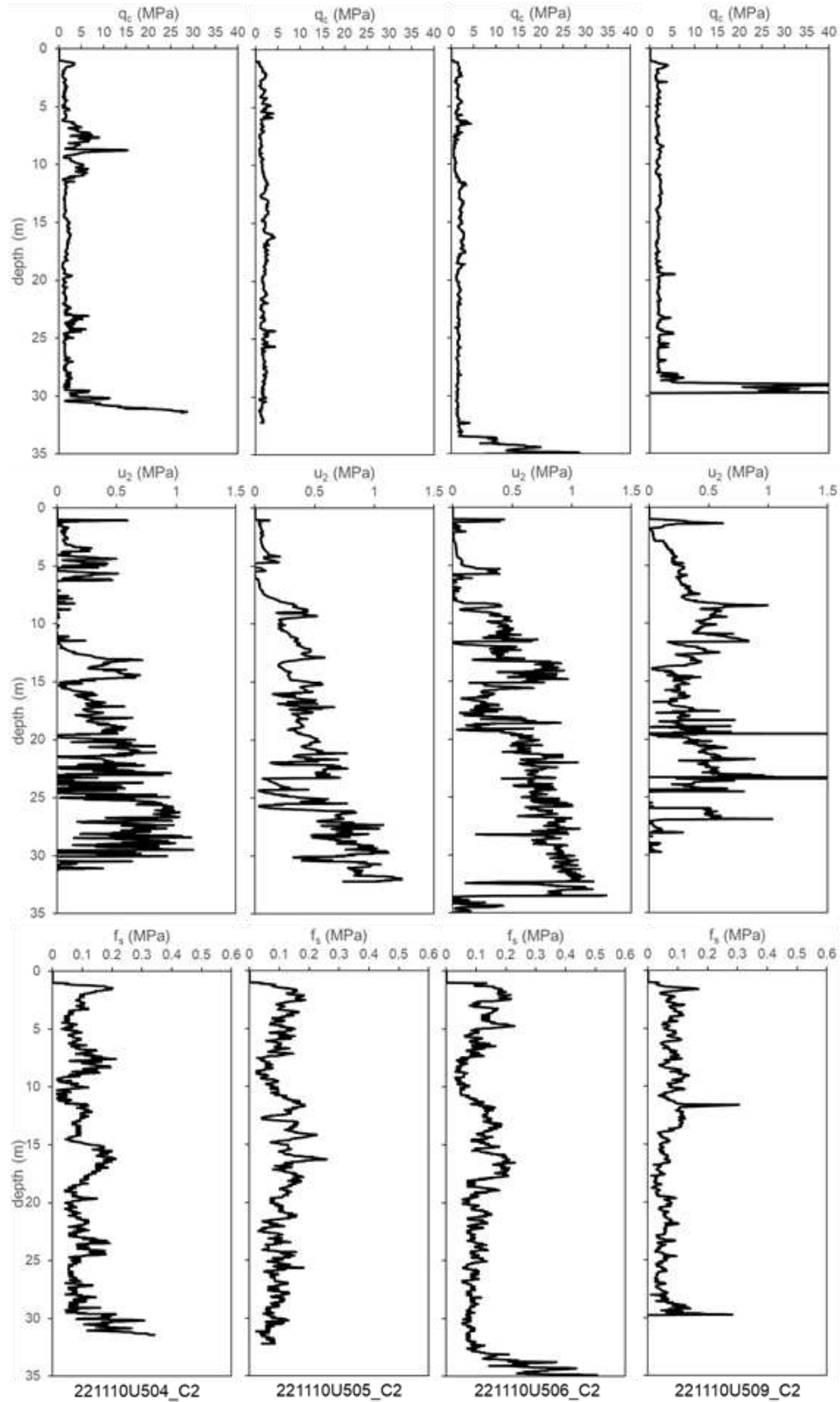


Figure 6. CPTu profiles ( $q_c$ ,  $u_2$ , and  $f_s$ ) related to Cluster 2 in Figure 1. From left to right: 221110U504, 221110U505, 221110U506, and 221110U509 CPTus in the attached database.

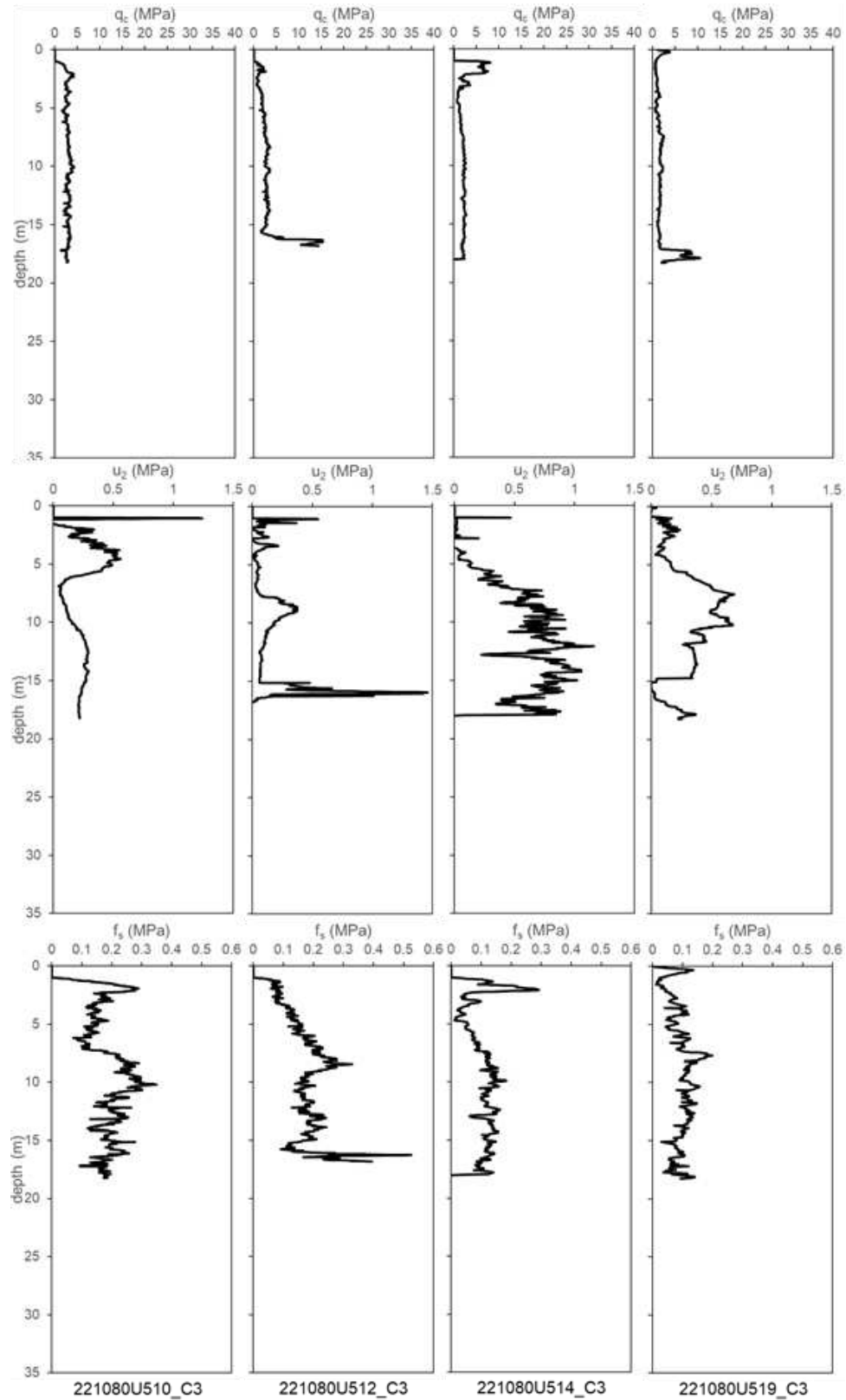


Figure 7. CPTu profiles ( $q_c$ ,  $u_2$ , and  $f_s$ ) related to Cluster 2 in Figure 1. From left to right: 221080U510, 221080U512, 221080U514, and 221080U519 CPTus in the attached database.



## METHODOLOGICAL APPROACH

### Geostatistical Analysis

To estimate the three-dimensional spatial distribution of  $q_c$ ,  $f_s$ , and  $u_2$ , while simultaneously providing quantification of the associated uncertainty, the Co-Kriging has been taken into account. Compared with other univariate techniques, this multivariate approach has the advantage of optimizing the estimation process by assuming spatial dependency among all the different considered variables (Castrignanò et al., 2000; Wackernagel, 2003; Webster and Oliver, 2007; Castrignanò, 2011). Among all the configurations of Co-Kriging, which are based on how the variables have been collected throughout the study area, this case is represented by the Partially Heterotopic configuration, i.e., when only some measurements are taken at the same locations. For this reason, we will refer throughout the text to our methodological approach by the name Partially Heterotopic Co-Kriging (PHCK).

As for the ordinary version of Co-Kriging, PHCK requires the definition of a Linear Model of Coregionalization (LMC) to reproduce the spatial dependency among the considered variables, where the results of independent physical processes occur on different scales (Castrignanò et al., 2015; Di Curzio et al., 2019; Vessia et al., 2020b). The LMC is modeled as a linear combination of  $N_S$  basic variogram functions, based on  $N(N + 1)/2$  experimental direct variograms and cross-variograms. In matrix notation, the LMC equation can be written as follows:

$$\mathbf{\Gamma}(\mathbf{h}) = \sum_{u=1}^{N_S} \mathbf{B}^u g^u(\mathbf{h}) \quad (3)$$

where  $\mathbf{\Gamma}(\mathbf{h})$  is an  $\mathbf{n} \times \mathbf{n}$  matrix of direct variograms (diagonal elements) and cross-variograms (non-diagonal elements), while  $\mathbf{B}^u$  is a symmetric matrix of coefficients  $b_{ij}^u$ , that represent the spatial structures  $g^u(\mathbf{h})$  related to each spatial scale  $u$ .

Direct variograms  $\gamma(\mathbf{h})$  is a spatial dependency function related to a given random function  $Z$ , that measures the variance of differences related to a separation vector called lag ( $\mathbf{h}$ ). Eq. (4) represents it below:

$$\gamma(\mathbf{h}) = \frac{1}{2N(\mathbf{h})} \sum_{i=1}^{N(\mathbf{h})} [z(\mathbf{x}_i) - z(\mathbf{x}_i + \mathbf{h})]^2 \quad (4)$$

where  $\mathbf{x}_i$  is the sampling location, while  $i = 1, \dots, N(\mathbf{h})$  indicates the set of  $N(\mathbf{h})$  pairs of sampling locations separated by a specific value of  $\mathbf{h}$ .

On the other hand, cross-variograms ( $\gamma_{z_i, z_j}(\mathbf{h})$ ) measure the joined variability of two variables  $z_i(\mathbf{x}_\alpha)$ s and  $z_j(\mathbf{x}_\alpha)$ , and are defined by the following Eq. (5):

$$\gamma_{z_i, z_j}(\mathbf{h}) = \frac{1}{2N(\mathbf{h})} \sum_{\alpha=1}^{N(\mathbf{h})} \{ [z_i(\mathbf{x}_\alpha) - z_i(\mathbf{x}_\alpha + \mathbf{h})][z_j(\mathbf{x}_\alpha) - z_j(\mathbf{x}_\alpha + \mathbf{h})] \} \quad (5)$$

where  $\mathbf{x}_\alpha$  is the location of the sampling point, and  $\alpha = 1, \dots, N(\mathbf{h})$  indicates the set of  $N(\mathbf{h})$  pairs of sampling locations separated by a specific value of  $\mathbf{h}$ , as already defined for direct variograms.

The estimation of each of the variables (i.e.,  $q_c$ ,  $f_s$ , and  $u_2$ ) within the considered domain has been performed through the following Eq. (6):

$$z_{i_0}^*(\mathbf{x}_0) = \sum_{i=1}^n \sum_{\alpha=1}^{n_i} \lambda_{\alpha}^i z_i(\mathbf{x}_\alpha) \quad (6)$$

where  $z_{i_0}^*(\mathbf{x}_0)$  is the target variable,  $i$  is the index of the variable, and  $\alpha$  it the location index. The estimation uncertainty can be quantified as well by the PHCK estimation variance ( $\sigma^2(\mathbf{x}_0)$ ), that is calculated by Eq. (7):



$$\sigma^2(\mathbf{x}_0) = 2 \sum_{i=1}^n \sum_{\alpha=1}^{n_i} \lambda_{\alpha}^i Y_{i\alpha}(\mathbf{x}_{\alpha}, \mathbf{x}_0) \sum_{j=1}^n \sum_{\beta=1}^{n_j} \lambda_{\beta}^j Y_{j\beta}(\mathbf{x}_{\beta}, \mathbf{x}_0) - Y_{i_0}(\mathbf{x}_0, \mathbf{x}_0) \quad (7)$$

The LMC described by Eq. (3) enables calculating the weights  $\lambda_{\alpha}$  in Eq. (6) and (7) through the Kriging equation system. Since PHCK is a stationary multivariate technique, Eq. (7) is considered meaningful only when the measured datasets have a Gaussian distribution. As a matter of fact,  $q_c$ ,  $f_s$ , and  $u_2$  variables are characterized by definitely non-Gaussian distributions, as is pointed out in Table 1(C3). To make the estimated variance values quantitative effective measures of uncertainty, all the considered variables have been transformed into Gaussian variables  $Y$  through the function named Gaussian Anamorphosis. This function is also able to convert a Gaussian variable  $Y$  into a new non-Gaussian distributed variable  $Z = \Phi(Y)$ , through a polynomial expansion fitting (Chilès and Delfiner, 2009):

$$\Phi(Y) = \sum \Psi_i H_i(Y) \quad (8)$$

where  $H_i(Y)$  are the Hermite polynomials, while  $\Psi_i$  represents the corresponding coefficients.

Starting from this function, a non-Gaussian variable is transformed into a Gaussian one by inverting the Gaussian Anamorphosis:

$$Y = \Phi^{-1}(Z) \quad (9)$$

The  $q_c$ ,  $f_s$  and  $u_2$  estimations have been performed by the ISATIS software (<https://www.geovariances.com/en/software-geovariances>; Geovariances, 2017).

Additionally, the best LMC has been selected through the Cross Validation procedure (Vessia et al. 2020a). It consists of calculating statistics from the output dataset values such as: the Mean Error (ME) and Root Mean Squared Error (RMSE), defined by Cressie (2015) as follows:

$$ME = \frac{1}{N} \sum_{i=1}^N (z(x_i) - z^*(x_i)) \quad (10)$$

$$RMSE = \sqrt{\frac{1}{N} \sum_{i=1}^N (z(x_i) - z^*(x_i))^2} \quad (11)$$

where  $N$  = number of data points,  $z(x_i)$  = sample data, and  $z^*(x_i)$  is the estimate at the sample point  $x_i$  from the  $N-1$  remaining sample data.

These variables measure the estimation bias and the precision, respectively. The optimal values of these statistics should be close to zero. Furthermore, the number of outliers is usually helpful to evaluate the estimation reliability.

### Model Uncertainty Quantification

To make the uncertainty calculated by Eq. (7) easily exploitable, the specific indexes proposed by Vessia et al. (2020a) have been used to build 3D error models: the Underestimation Error (UE%) and the Overestimation Error (OE%) percentages:

$$UE\% = \frac{|z(x) - LL|}{z(x)} \% \quad (12)$$



---

$$OE\% = \frac{|z(x) - UL|}{z(x)}\% \quad (13)$$

where LL and UL are the lower (LL) and upper (UL) limits of the 95% confidence interval of the Gaussian transformed estimates, for each one of the selected variables.

### QUANTITATIVE 3D MECHANICAL SUBSOIL MODELS

Based on the spatial variability structures drawn from the sampling semivariograms fitted by means of nested spherical semivariogram models, the horizontal and vertical variability structure of the data  $q_c$ ,  $f_s$  and  $u_2$  have been calculated, as shown in Figure 8.

The variograms and cross-variograms of the LMC (Figure 8) have been built based on the entire dataset, meaning that all 182 CPTus measurements have contributed. The dataset has been considered as a whole, so its spatial variability structures were modeled through an anisotropic LMC: one isotropic structure on the horizontal plane and one vertical structure. Each of these structures is not simple but nested; i.e., more than one basic spatial variability structure is used to fit the data. Every basic structure is characterized by a range and a partial sill, which can be considered to thoroughly describe complex spatial patterns typical of such soil mixtures. Provided that the PHCK is a stationary method, Gaussian distributed datasets are needed. Thus, the raw measurements have been properly transformed into standardized values through the Gaussian Anamorphosis function, referred to by a prefix “g”. At the end of the calculation process, the standardized estimated variables have been back-transformed, changing the prefix “g” into “k”.

Calculated variograms and cross-variograms reveal that the most correlated measured parameters are  $q_c$  and  $f_s$ , while  $u_2$  seems to not significantly affect the variability structures of the other two. This is true for both anisotropic variability structures. The vertical semivariograms of  $q_c$  and  $u_2$  show a non-stationary trend that has been modeled by the k-Bessel semivariogram structure. The k-Bessel function models those spatial variability structures that show long-range stationarity. Such variability structures have been used to interpolate the data into continuous 3D  $q_c$ ,  $f_s$ , and  $u_2$  models by means of the PHCK.

Different 3D models of continuous data for each variable have been calculated: the estimated value, the underestimation error, and the overestimation error. The  $q_c$  excavated solid model was shown in Figure 9, whereas in Figures 10 and 11 present the lower and upper error values. From the 3D model of the estimated values, bodies of higher tip resistance that are paleo-channel areas can be seen. These bodies are quite extended but not layered. Thus, it could be difficult to recognize these inclusions without using a continuous model. Errors, as Figures 10 and 11 illustrate, happen at a rate of about 30-40%, although they increase at the edges of the domain due to the lack of data or wherever the gravel bodies are detected. The influence of the gravel bodies on the errors of  $f_s$  is less evident because it is a smoothed variable (Figures 12, 13, and 14). Additionally, the Co-Kriging operator is well known to smooth the sharp spatial variations in the estimation process.

To assess the LMC performance, the ME and RMSE values have been calculated through cross-validation, as listed in Table 3. The selected LMC clearly appears to be unbiased and precise because both the ME and RMSE values are almost zero.

*Table 3. ME and RSME values from cross-validation related to the Gaussian transformed  $q_c$  and  $f_s$  variables.*

| Variable | ME       | RMSE   |
|----------|----------|--------|
| gfs      | 0.000370 | 0.1789 |
| gqc      | 0.000001 | 0.1676 |

In detail, Figure 16 illustrates the 3D  $q_c$  model of a portion of the Imola municipality at different depths under the surface level (i.e., at 5, 10, 15, and 20 m). From this model, the local increases of the tip resistance value are shown and can be followed along with depth, as well as at a fixed depth throughout the considered area. It is worth emphasizing the ability of this data model to deal with the multiscale heterogeneity of the subsoil; if further CPTs will be locally added to the model, not only will this increase our knowledge of the mechanical properties of the soils but also the quality of the estimates. In other words, the calculated uncertainty could be reduced even to estimates far from the location of the new investigation. The PHCK technique uses all the measures of the dataset to calculate both estimates and uncertainties; however, the farther they are, the less their influence in the calculation at each model point.

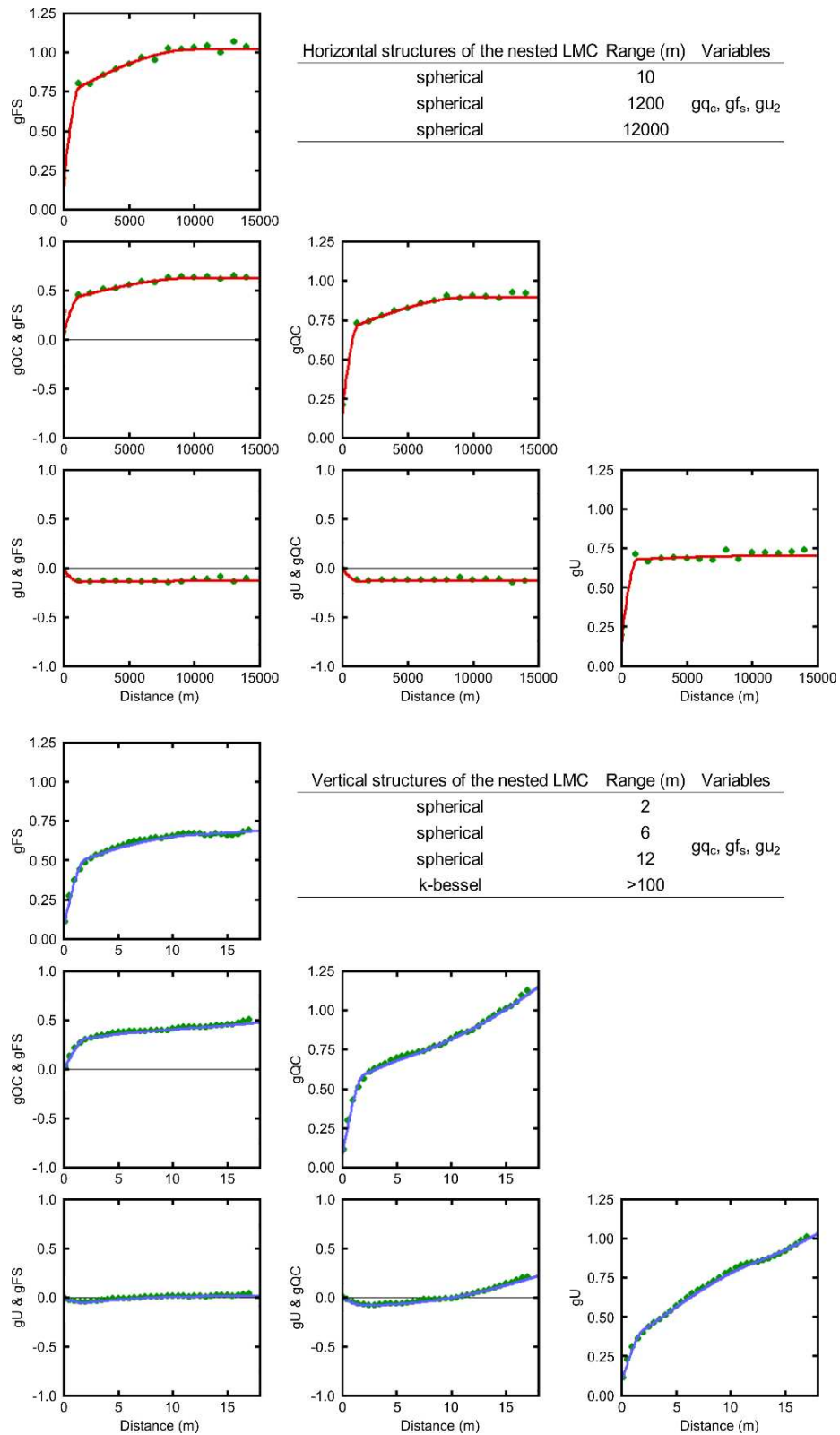


Figure 8. Linear Model of Coregionalization related to the Gaussian transformed  $f_s$ ,  $q_c$ , and  $u_2$  variables. The green dots are the experimental values, while the blue and red lines are the model lines of direct variograms and cross-variograms (the red lines relate to the horizontal model, while the blue lines relate to the vertical model).

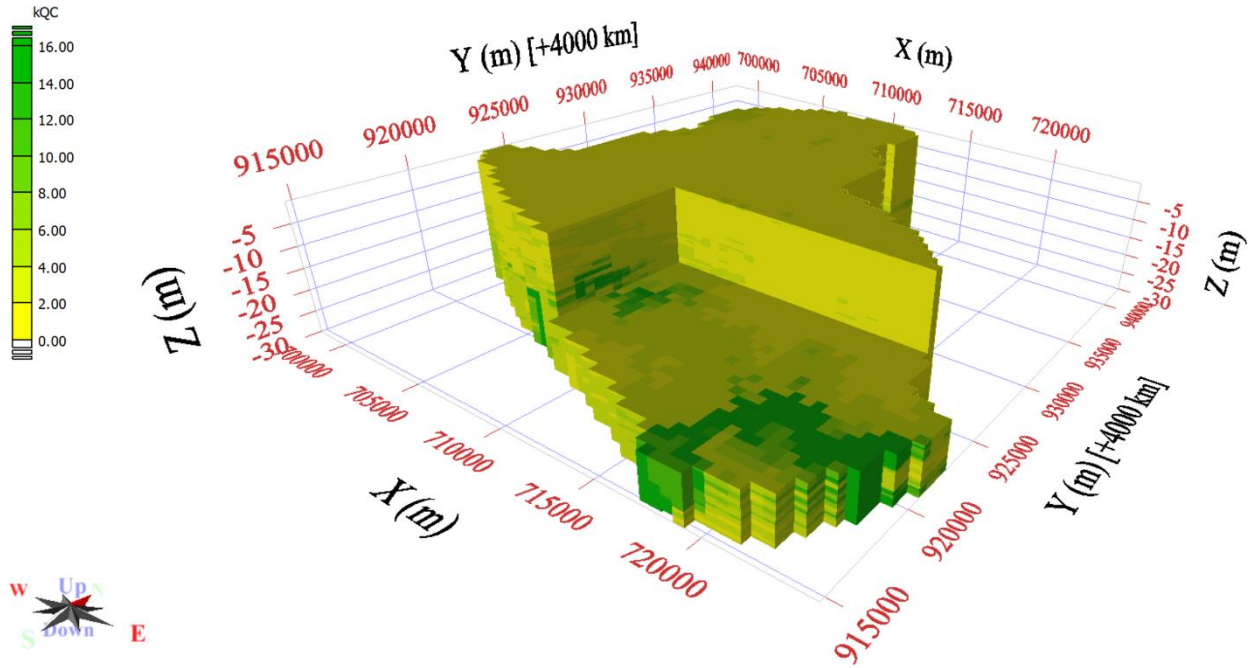


Figure 9. 3D excavated solid model of  $q_c$  estimated values.

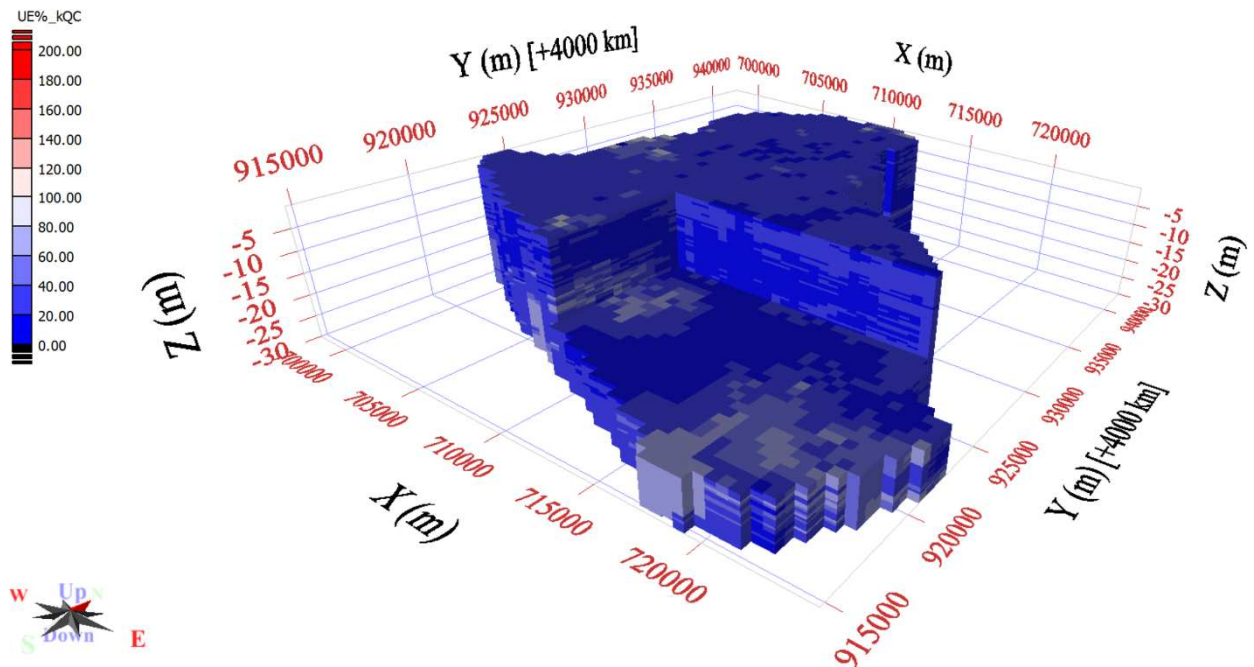


Figure 10. 3D excavated solid model of  $q_c$  underestimated error.

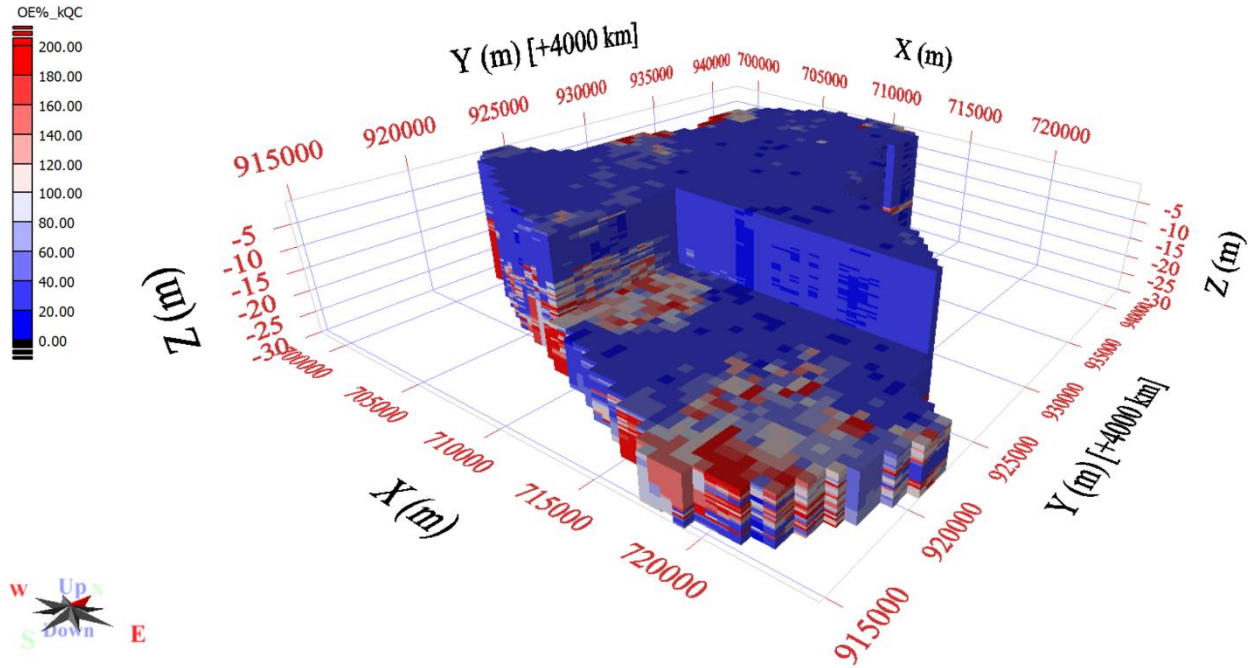


Figure 11. 3D excavated solid model of  $q_c$  overestimated error.

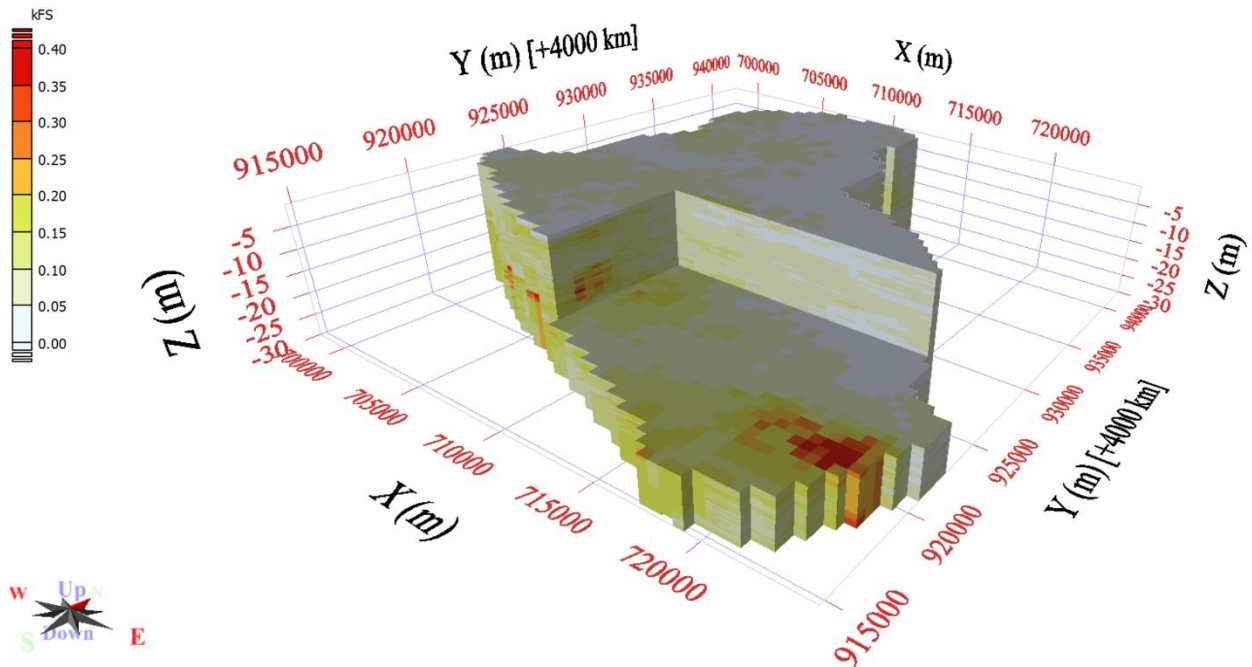


Figure 12. 3D excavated solid model of  $f_s$  overestimated error.

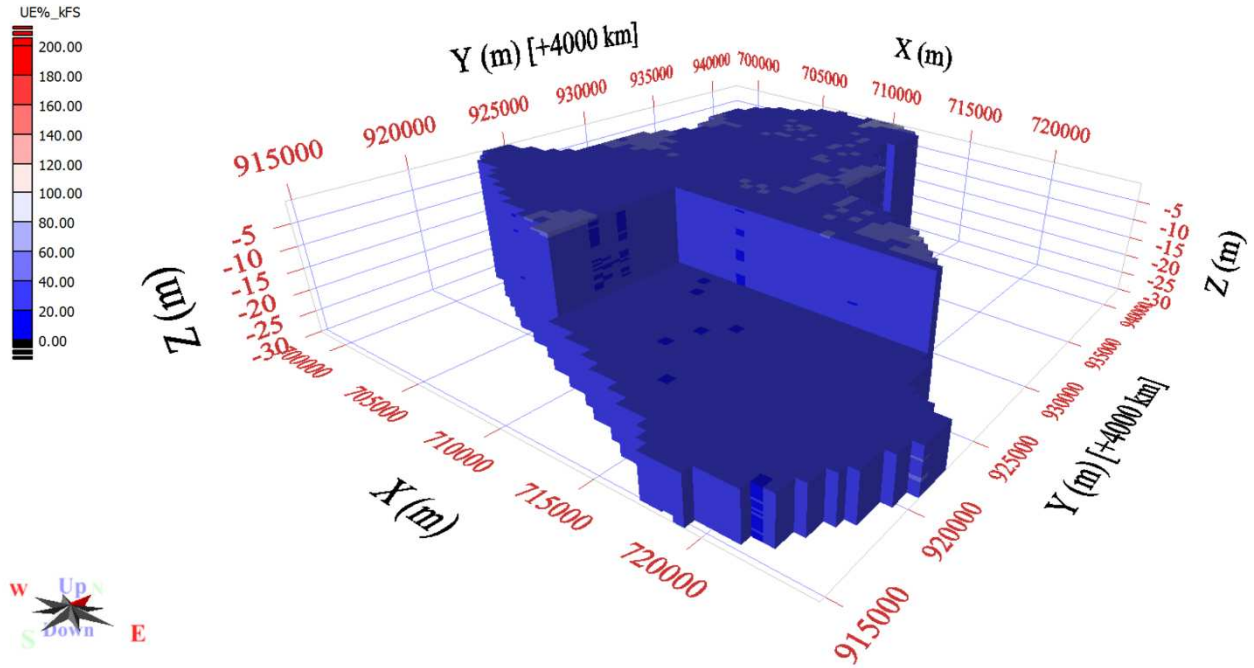


Figure 13. 3D excavated solid model of fs underestimated error.

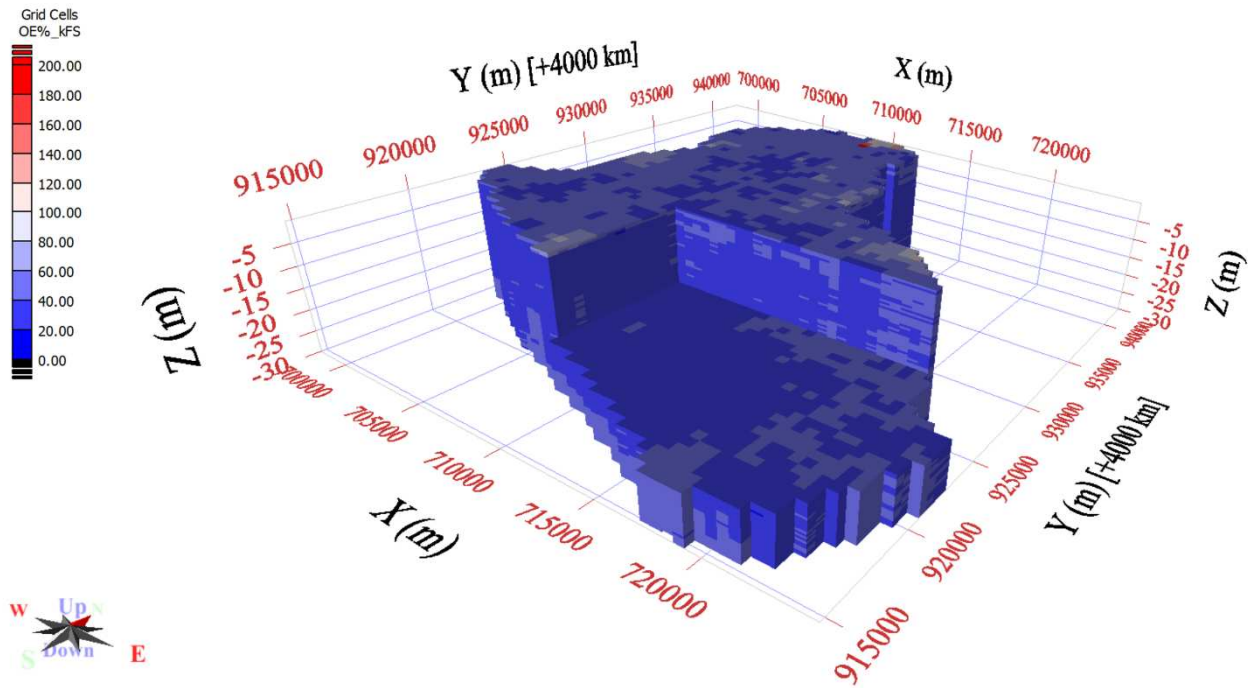


Figure 14. 3D excavated solid model of fs overestimated error.

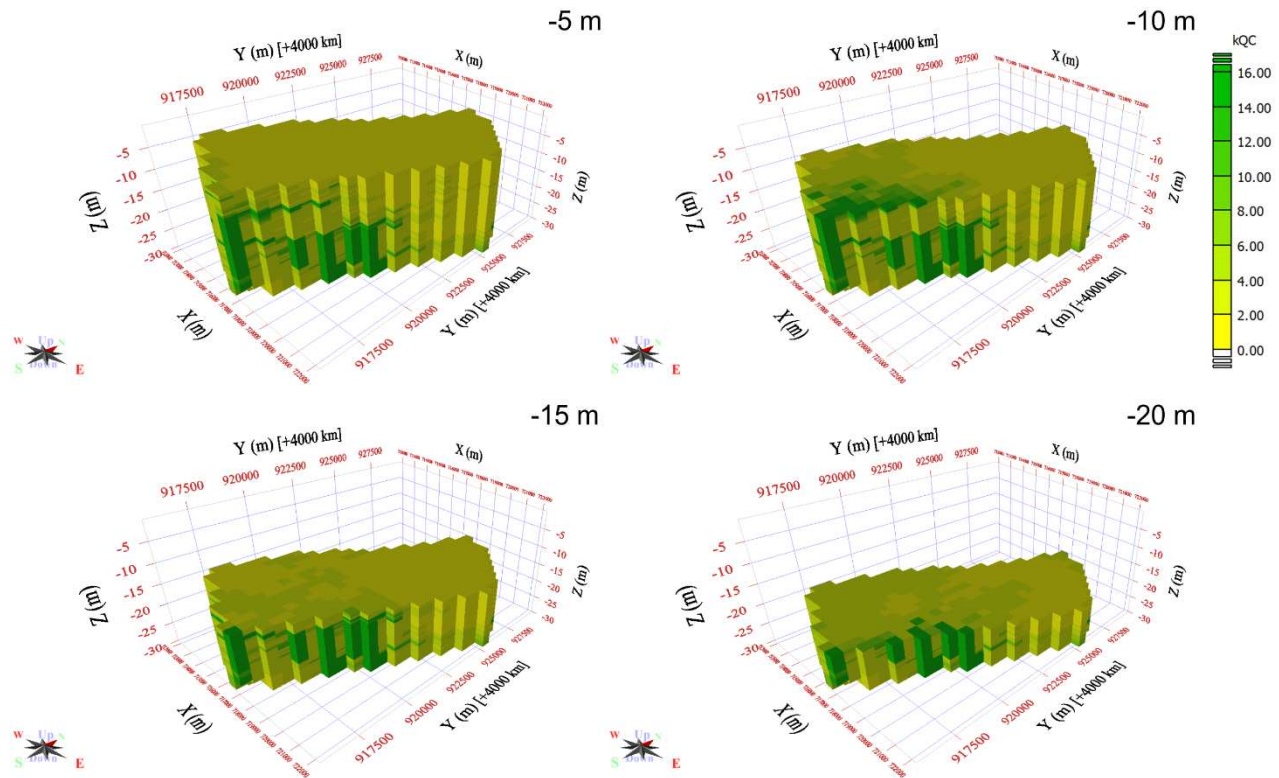


Figure 15. 3D model of  $q_c$  of a portion of the Imola municipality, sliced at different depths. Its location is shown in Figure 1.

## CONCLUSIONS

The geostatistical tools can be very useful in reconstructing 3D continuous data models of mechanical measured parameters, such as those from CPTus. The Partially Heterotopic Co-Kriging technique proved to be a powerful method to interpolate individual investigations even at a large distance and to generate continuous data volume of the subsoil wherever numerous profiles can be handled as georeferenced data. This type of data management can be timesaving and promises to reduce the financial demands in planning and designing activities because it advantageously enables, among other things, the recognition of those areas where supplementary investigations are required as well as where increases or decreases in soil resistances are expected. Some work is still needed to integrate the resultant solid data models within BIM (Building Information Modeling) and GIS (Geographic Information System) environments.

## ACKNOWLEDGMENTS

The authors are grateful to Dr. Luca Martini from the Regional Office for Territorial Protection and Development of the Emilia-Romagna Region for providing the dataset.

## REFERENCES

- Amorosi, A., and Farina, M. (1995). "Large scale architecture of a thrust-related alluvial complex from subsurface data: the Quaternary succession of the Po basin in the Bologna area (Northern Italy)." *Giorn. Geol.*, 57(1-2), 3-16.
- Castrignanò, A. (2011). "Introduction to spatial data processing." *Aracne editrice*, Roma.
- Castrignanò, A., Giugliarini, L., Risaliti, R., and Martinelli, N. (2000). "Study of spatial relationships among some soil physico-chemical properties of a field in central Italy using multivariate geostatistics." *Geoderma*, 97, 39-60.
- Castrignanò, A., Landrum, C., and De Benedetto, D. (2015). "Delineation of Management Zones in Precision Agriculture by Integration of Proximal Sensing with Multivariate Geostatistics." *Examples of Sensor Data Fusion Agric.*, 80, 39-45.



- 
- Chilès, J.-P., and Delfiner, P. (2012). *Geostatistics: Modeling Spatial Uncertainty, 2nd ed.*, Wiley, Hoboken, NJ, USA.
- Cressie, N. (2015). *Statistics for spatial data, Revised Edition*, Wiley Classical Library, New York.
- Di Curzio, D., Rusi, S., and Signanini, P. (2019). “Advanced redox zonation of the San Pedro Sula alluvial aquifer (Honduras) using data fusion and multivariate geostatistics”. *Sci. Total Environ.*, 695.
- ISPRA (2009a). *Carta Geologica d'Italia (scala 1:50000), Foglio 221 «Bologna»*, Servizio Geologico d'Italia, SystemCart s.r.l, Roma.
- ISPRA (2009b). *Carta Geologica d'Italia (scala 1:50000), Foglio 239 «Faenza»*, Servizio Geologico d'Italia, SystemCart s.r.l, Roma.
- Pieri, M., and Groppi, G. (1981). *Subsurface Geological Structure of the Po Plain, Italy*, Pubbl. 414 P.F. Geodinamica, CRN. Regione Emilia-Romagna and ENI-AGIP (1998). *Riserve idriche sotterranee della Regione Emilia Romagna*, G. Di Dio, E. El. Ca. (eds.), Firenze.
- Robertson, P. K. (2009). “CPT interpretation – a unified approach.” *Canadian Geotech. J.*, 46, 1-19.
- Vessia, G., Di Curzio, D., and Castrignanò, A. (2020a). “Modeling 3D soil lithotypes variability through geostatistical data fusion of CPT parameters.” *Sci. Total Environ.*, 698.
- Vessia G., Di Curzio D., Chiaudani A., and Rusi S. (2020b). “Regional rainfall threshold maps drawn through multivariate geostatistical techniques for shallow landslide hazard zonation.” *Sci. Total Environ.*, 70525, 135815.
- Wackernagel, H. (2003). *Multivariate Geostatistics: An Introduction with Applications*, Springer-Verlag, Berlin.
- Webster, R., and Oliver, M.A. (2007). *Geostatistics for Environmental Scientists*, John Wiley & Sons, New York.



# INTERNATIONAL JOURNAL OF GEOENGINEERING CASE HISTORIES

*The Journal's Open Access Mission is  
generously supported by the following Organizations:*



Access the content of the *ISSMGE International Journal of Geoengineering Case Histories* at:  
[www.geocasehistoriesjournal.org](http://www.geocasehistoriesjournal.org)